J Mater Sci (2010) 45:662–668
DOI 10.1007/s10853-009-3983-9

Microstructure and property characterisation of 3-3 Al(Mg)/Al_2O_3 interpenetrating composites produced by a pressureless infiltration technique

Hong Chang · Rebecca Higginson · Jon Binner

Received: 5 June 2009 / Accepted: 13 October 2009 / Published online: 24 October 2009

Abstract 3-3 Interpenetrating composites, consisting of 3-dimensionally interpenetrating matrices of two different phases, are interesting materials with potentially superior properties when compared with traditional metal matrix composites. In the present research, gel-cast Al_2O_3 foams with open porosity in the form of spherical cells connected by circular windows were pressurelessly infiltrated using an Al-8 wt% Mg alloy. Electron backscatter diffraction (EBSD) analysis revealed that the alloy had a large grain size with single grains generally inhabiting multiple cells. The flexural strength of the composites, tested using 3-point bending, was ~350 MPa, rather high when compared to other Al-alloy-based Al_2O_3 composites. The strength increased with both decreasing foam density and cell size. The reasons for the high strength are good metal–ceramic interfacial bonding, crack bridging by plastic deformation of the metal phase and crack deflection.

Introduction

It is well known that the majority of metal–ceramic composites exhibit superior fracture toughness and damage tolerance when compared to monolithic ceramics. A dominant toughening mechanism is believed to be crack bridging by ductile metal ligaments, which provides closure forces in the crack wake, thereby reducing the crack tip stress [1]. In addition to crack bridging, crack deflection [2] and process zone shielding [3] are other possible toughening mechanisms, although their effects are believed to be smaller [4, 5]. A study on the mechanical properties of hot-pressed Al_2O_3/NiAl composites showed that the toughening effect was a combination of crack deflection and crack bridging due to the presence of weak Al_2O_3/NiAl interfaces and the interconnected NiAl particles. The increase in the strength observed was partly attributed to the microstructural refinement of the composite [6].

Amongst the metal–ceramic composites, Al and its alloys, reinforced with ceramic particles [7–10], fibres [11] or intermetallic particles [12] are materials in high-performance applications due to their superior properties. Commercial approaches to producing these composites generally involve stirring particles into molten metals followed by casting or infiltrating densely packed beds of either particles or fibres. Unlike the traditional composites, where the matrix contains either a completely disconnected phase (0-3) or, if continuous fibres are used, a dispersed phase connected in a single direction (1-3), interpenetrating composites have both phases connected in all three dimensions (3-3), which can result in substantially different properties. Prielipp et al. [13] studied the mechanical properties of Al/Al_2O_3 interpenetrating composites produced by gas pressure infiltration of molten Al into Al_2O_3 preforms and reported strengths up to 810 MPa and fracture toughnesses up to 10.5 $MPam^{1/2}$; the Al contents were 25 and 35 vol.% with metal ligament diameters 0.08, 0.25, and 0.8 μm for each Al content. A study of Ni_3–Al/Al_2O_3 interpenetrating composites [14] showed that flexural strengths of ~700 MPa could be obtained in composites having 30 vol.% of Ni_3Al; however, with decreasing Ni_3Al content the flexural strength decreased to 300–400 MPa (Ni_3Al contents <25 vol.%). Delamination between the ceramic and the Ni_3Al was a possible cause for the low fracture strength in the latter. Klassen et al. [15] investigated Nb–Al/Al_2O_3 composites containing 54–70 vol.%

H. Chang (✉) · R. Higginson · J. Binner
Department of Materials, Loughborough University, Loughborough LE11 3TU, UK
e-mail: Hong.chang@nottingham.ac.uk

Al_2O_3 with an interpenetrating microstructure and found that the flexural strength of the composites could be enhanced to ~520 MPa and fracture toughness values of 5.74 $MPam^{1/2}$ were obtained.

Although 3–3 connectivity is fairly common in natural composites, e.g. bones and wood, the difficulty with synthesising a truly interpenetrating network lies in achieving the required connectivity and spatial distribution of the phases, especially on a fine scale [16]. However, the ability to fabricate by design such an interpenetrating microstructure raises the possibility of developing materials with truly multifunctional properties, each phase contributing its own characteristics to the macroscopic properties of the composite. One route to achieve tailorable 3–3 composites is via the infiltration of a second phase into porous materials that display complete pore interconnectivity; provided that the structure of the initial porous material can be controlled sufficiently in terms of the degree of porosity, the size and shape of the cells, the size of the windows between them and the nature of the struts separating them, then there is the opportunity to design and fabricate interpenetrating composites with customised structures [17]. This research considers the microstructure and flexural property of Al(Mg)/Al_2O_3 interpenetrating composites produced using a pressureless infiltration technique. The fractured composites were thoroughly studied and the correlations between the composite microstructure, e.g. foam density and cell size, and the composite properties are discussed.

Experimental

Al_2O_3 foams were supplied by Dyson Thermal Technologies (Dyson TT), Sheffield, UK. Samples measuring 70 mm × 20 mm × 10 mm having foam densities of 15–35% of theoretical and cell sizes in the range of 50–160 μm, were gel cast from an aqueous suspension of Al_2O_3 powders of two grades: 0.5 and 6 μm with a ratio of 10:1. An Al-8 wt% Mg alloy, selected on the basis of previous research [17], was used as the infiltrant. Full details of the composite manufacture are described elsewhere [17, 18]; however in brief, the Al_2O_3 foam rectangles were placed on top of alloy slices in alumina boats, which were heated at 20 °C min^{-1} in Ar in a tube furnace. Once the temperature reached 915 °C the gas was switched to N_2; a holding time of 30 min in N_2 was adopted for complete infiltration. Our research showed that excessive exposure to N_2 using it throughout the entire heat treatment cycle led to the formation of excess AlN at the metal–ceramic interfaces, whilst insufficient exposure to N_2 prevented infiltration.

The composites, which were based on foams of different densities and cell sizes, were cut longitudinally into 35 mm × 4 mm × 3 mm bars for 3-point bending; the tensile surface was polished using 6-μm diamond paste and the edges were chamfered at 45°. The flexural strength was measured at a cross-head speed of 0.5 mm/min with a span width of 20 mm.

For microstructure observation, samples were prepared using standard metallographic techniques and observed using a LEO VP 1530 field emission gun scanning electron microscope (FEG SEM) equipped with TSL electron backscatter diffraction (EBSD). Samples for EBSD analysis were further polished using Ar^+ ion milling for 45 min at 5 kV and a gun tilt angle of 5° in a Gatan PIPS system. The fracture surfaces after the 3-point bend measurements were also observed using the FEG SEM. In addition, a FEI Dual Beam Nova 600 Nanolab focussed ion beam (FIB) and a JEOL JEM 2000FX TEM with an EDX system were used for preparing TEM samples and their observation, respectively.

Results and discussion

Microstructure

Figure 1a shows an EBSD phase map of the Al–Mg/Al_2O_3 interpenetrating composite; the composite was based on a 15% dense foam with an average cell size of 60 μm. It can be seen that the metal alloy completely infiltrated the foam. From Fig. 1b, the image quality/inverse pole figure of the composite, it can be observed that whilst the pattern quality obtained from both the ceramic and the alloy were good, the step size used in the scan was too coarse to yield full detail of the much finer Al_2O_3 microstructure. In general, the alloy present within groups of neighbouring cells had the same crystallographic orientation. This indicates that the alloy has large grains that inhabited a number of cells in the ceramic foam. The alloy tended towards (101) and (001) type orientations parallel to the infiltration direction, a result consistent with previous research [17]. From Fig. 1b, it may be observed that in the largest cells, marked as 'A' and 'B' in the figure, grain boundaries could be seen in the alloy, suggesting that there is an upper size limit for the alloy grain size when in particularly large ceramic foam cells. Previous research by the current authors has shown that the infiltrated metal within these large cells consisted of grains that nucleated preferentially on the cell walls with grain growth being reduced by contact with other grains and cell walls [19]. Similarly, when Zhao et al. [20] studied the solidification structure of squeeze cast Al alloy/SiC interpenetrating composites they found that primary α-Al dendrites formed first near the strut of the SiC foam and grew into the center of cell; with decreasing cell sizes, columnar α-Al dendrites perpendicular to the struts of the SiC foam were more easily formed.

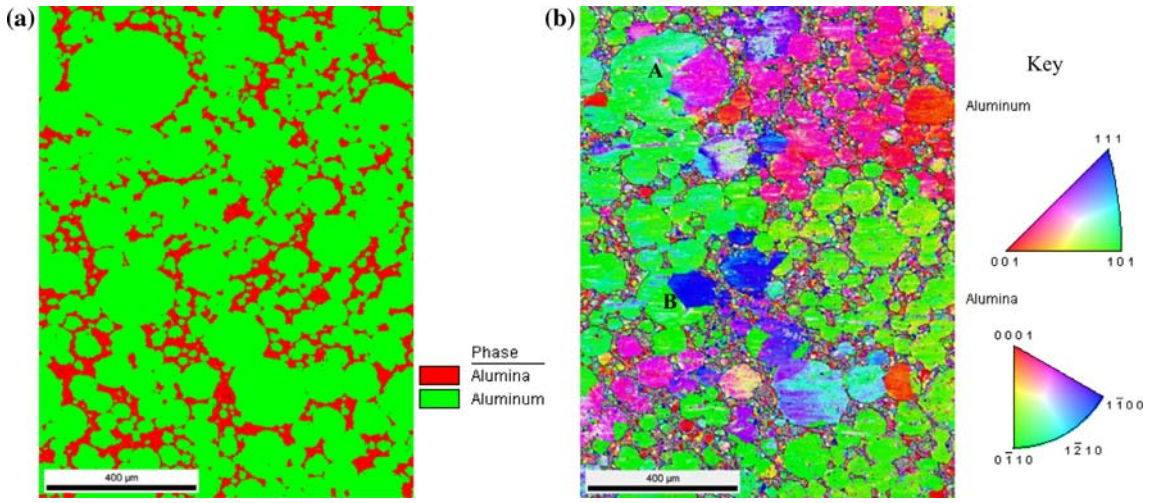

Fig. 1 EBSD analysis of the Al-8 wt% Mg/Al_2O_3 interpenetrating composites: **a** phase map, **b** image quality (IQ)/inverse pole figure (IPF)

Strength

Figure 2a, b shows the flexural strength of both the un-infiltrated foams and the composites, respectively. The former increases approximately linearly with increasing foam density; from ~5 to ~20 MPa with an increase in foam density from 15 to 35% of theoretical. In contrast, the flexural strength of the composites slightly decreased with increasing foam density, though the absolute values are much larger. With respect to the effect of cell size, the flexural strength of both the foams and the composites increased with decreasing cell size.

A study on pressurelessly infiltrated Mg–Al–Zn/Si_3N_4 interpenetrating composites [21] showed that with 6 vol.% Si_3N_4 in the Mg–Al–Zn alloy, the bending strength and fracture toughness were improved; however, with further increase of the Si_3N_4 content both the bending strength and the fracture toughness of the composite decreased. The flexural strength decreased from 280 to 240 MPa as the Si_3N_4 content increased from 6 to 15 vol%—similar to the effect of the foam density in Fig. 2b. Travitzky and Shlayen [22] studied pressurelessly infiltrated Al_2O_3/Cu–O alloy composites containing different volume fractions of open porosity and reported that the bending strength of the composites increased from 250 to 330 MPa with increasing metal content from 12.5 to 29 vol.%; crack bridging by the Cu–O alloy was the main toughening mechanism and underpinned the strength obtained.

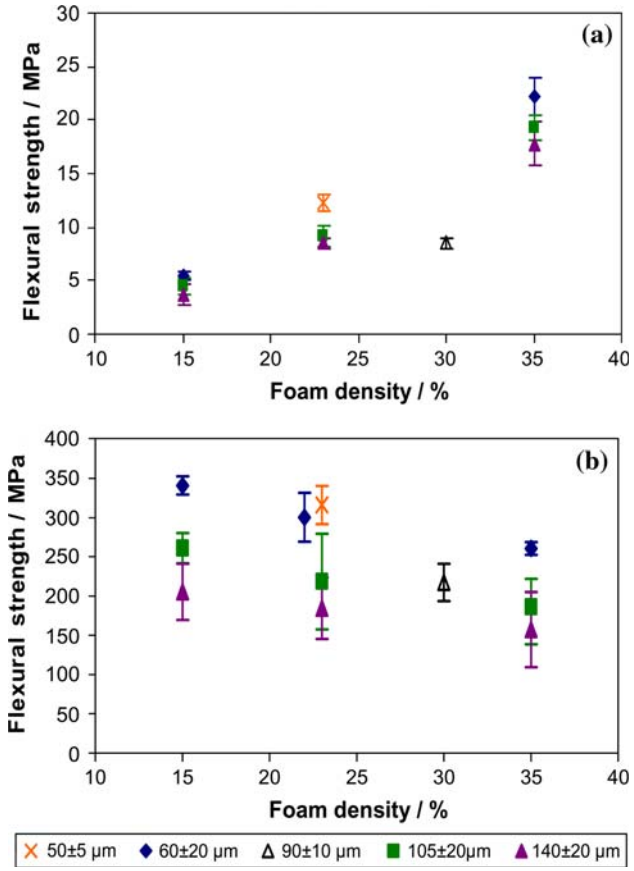

Fig. 2 Flexural strength of **a** the un-infiltrated Al_2O_3 foams and **b** the Al-8 wt% Mg/Al_2O_3 composites having different foam densities and cell sizes

Fracture surface

Figure 3 shows the fracture surface morphologies of the composites made from 15 and 23% dense foams with an average cell size of 60 and 140 μm, respectively. The micrographs were taken using both secondary electron microscopy and back-scattered electron microscopy. From Fig. 3a, the surface is rough and consists of spherical 'hills'; from Fig. 3b, the distributions of the metal and ceramic phases are clearly seen with plastic deformation of

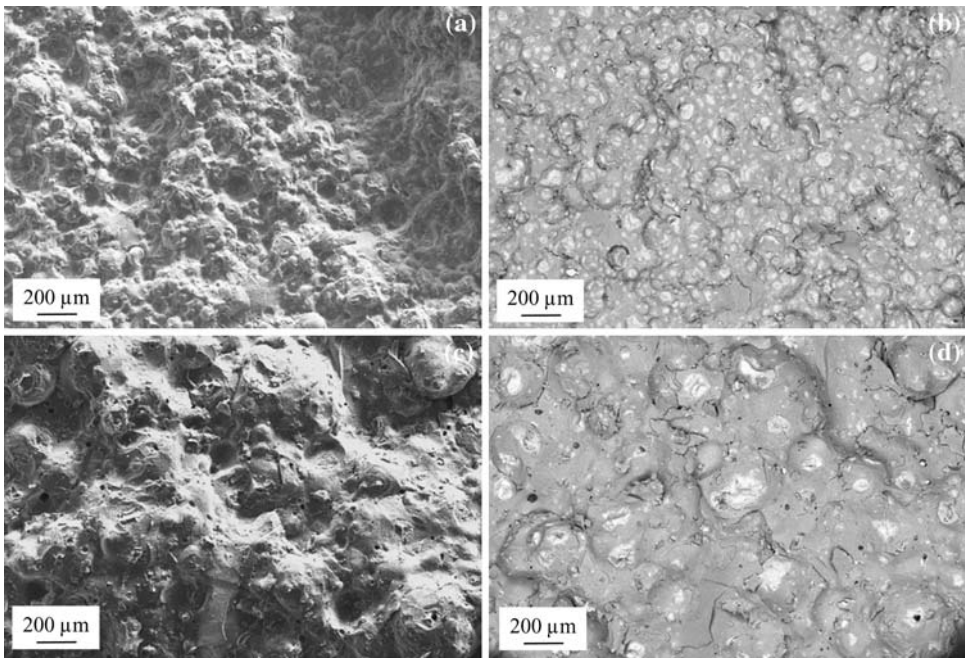

Fig. 3 SEM fracture micrographs of the Al-8 wt% Mg/Al_2O_3 composite: 15% dense foam with 60 µm cells **a** second electron microscopy, **b** back-scattered electron microscopy; 23% dense foam with 140 µm cells, **c** second electron microscopy, **d** back-scattered electron microscopy

the Al phase observed. The composite produced from the 23% Al_2O_3 foam, Fig. 3c, shows a much less rough fracture surface morphology than that in Fig. 3a due to the higher foam density and larger cell size (140 µm compared with 60 µm); a few pores are exposed on the fracture surface (Fig. 3d), which could be either closed pores in the foam struts or a result of metal shrinkage, especially at the Al 'dendritic' crystal ends.

Figure 4 shows typical micrographs of the composites at higher magnifications, where the metal phase was extensively deformed and finally, fractured, though the metal–ceramic interface was intact. From Fig. 4a, a crack 'A' is present in the ceramic phase ~20 µm away from the metal–ceramic interface illustrating good metal–ceramic interfacial bonding. From Fig. 4b it can be observed that the smaller Al_2O_3 grains fractured mainly intergranually, while transgranular fracture had occurred in the larger Al_2O_3 grains (A).

A TEM electron micrograph at the metal–ceramic interface of the composite after 3-point bending is shown in Fig. 5a; the TEM sample was taken ~2 mm away from the fracture tip on the tensile surface of the sample. The large Al_2O_3 grains at the top of the micrograph could either be intrinsic to the sample, i.e. part of the coarser 6-µm powder used, or a result of Al_2O_3 grain growth. Three vertical dislocations may be seen in the Al_2O_3 grain, though they were rarely observed. Little porosity was seen at the interface, which again indicates strong interfacial bonding.

An EDS line-scan analysis across the interface from the Al_2O_3 to the Al-8 wt% Mg alloy is shown in Fig. 5b. It may be observed that both the Mg and the N are concentrated in the interface layer, which can be divided into an Al–O–Mg region near the ceramic and an Al–N–O–Mg region near the Al alloy. To identify the interface compounds in more detail, TEM diffraction patterns were taken; hexagonal AlN was found in the Al–N–O–Mg region and cubic $MgAl_2O_4$ observed at discrete points in the Al–O–Mg region [18]. Although the aluminium alloy infiltrant contained 8 wt% Mg, from the EDS data, the Mg content in the alloy after infiltration was ~6 wt% whilst

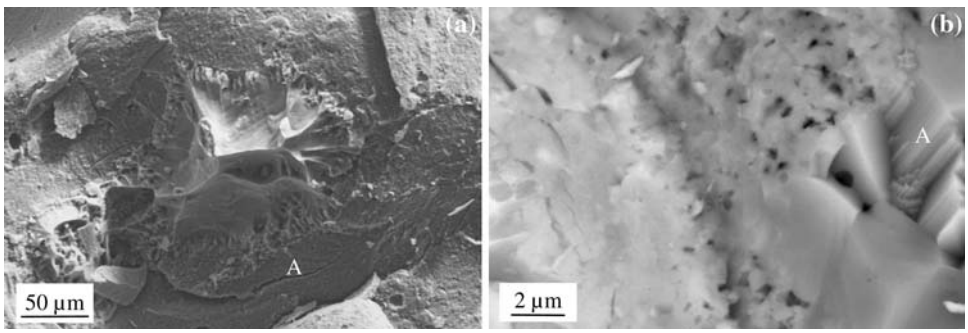

Fig. 4 SEM micrographs of the fracture surfaces of the Al-8 wt% Mg/Al_2O_3 composite: **a** 15% foam density, 60 µm average cell diameter; **b** 23% foam density, 140 µm average cell diameter

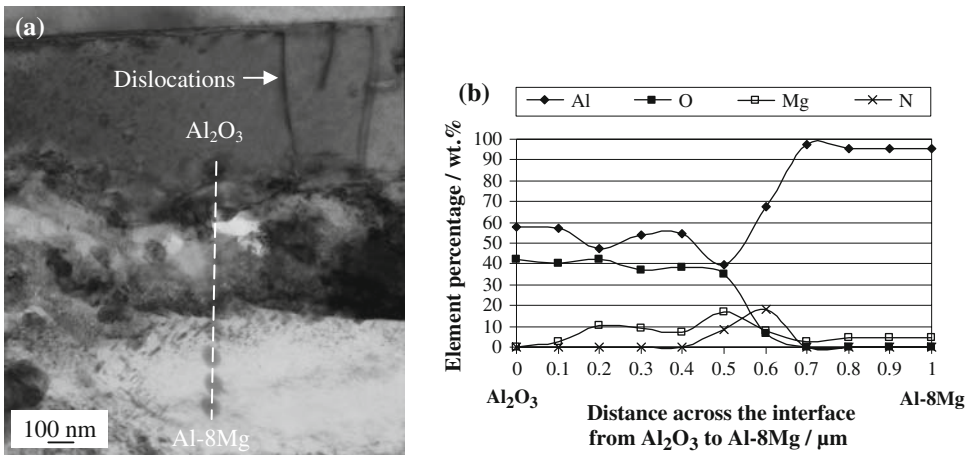

Fig. 5 TEM micrograph and EDS line-scan analysis of the Al-8 wt% Mg/Al_2O_3 composite at the metal–ceramic interface: **a** the line-scan position, **b** the EDS result

there was ~10 wt% Mg in the metal–ceramic interface layer. Our previous research has shown that Mg evaporates from the molten alloy and deposits onto the surface of the Al_2O_3 foam, this is a key stage in improving the wettability between the molten alloy and the Al_2O_3 foam and results in the spontaneous pressureless infiltration. The process occurs via a two-step nitridation mechanism through which the Mg is recycled. This explains the reduction in the Mg content in the alloy and the presence of increased levels of Mg in the interface layer. The TEM analysis [18] suggests that the Mg can react with the Al_2O_3 to form $MgAl_2O_4$ or, if in significant local excess, it can form MgO.

Crack propagation

A typical micrograph of a crack propagation route observed on the compression surface of one of the Al(Mg)/Al_2O_3 samples is shown in Fig. 6. It can be seen that the crack propagated preferentially through the brittle ceramic phase; when it encountered the ductile metal, the metal deformed and the crack was bridged by the metal. In addition to the metal bridging, crack deflection in the ceramic phase is also visible, explaining the fracture surface morphologies in Fig. 3.

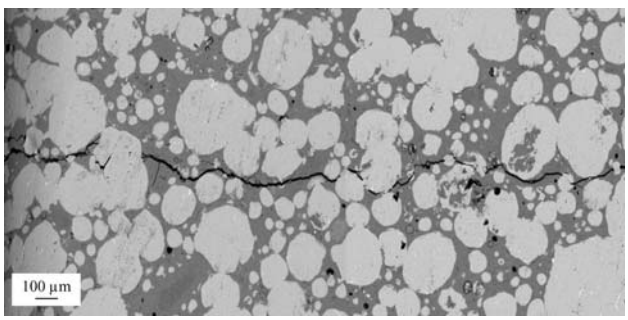

Fig. 6 Back-scattered electron micrograph of the crack propagation route of an Al-8 wt% Mg/Al_2O_3 composite. The Al_2O_3 foam infiltrated was 23% dense with an average cell size of 105 μm

Another micrograph of the crack propagation at a higher magnification is shown in Fig. 7a. The metal deformation, crack propagation in the ceramic phase and crack deflection, are all clearly visible. Due to the large grain size of the Al phase, plastic deformation could have occurred within a group of neighbouring cells. As is shown in Fig. 7b, slip bands are observed in the alloy in two neighbouring cells. This indicate that the single crystal structure of the alloy in this region, associated with strong metal–ceramic interfacial bonding, enabled a larger volume of deformation; hence, absorbing more energy than that could have been achieved if each cell had contained an independent metal grain. Some composites tested in the current study did not completely separate after the 3-point bending measurement, especially for those containing greater metal contents, due to the presence of the single crystallographic Al grains and the occurrence of Al deformation and crack bridging.

Effect of foam characteristics

From Fig. 2b, the composites displayed higher flexural strength with both lower ceramic foam densities and smaller foam cell sizes. The former is related to the higher content of the ductile metal phase, which plays an important role in bridging the cracks via plastic deformation and absorbing the energy as outlined above; the latter is related to a finer microstructure. As the foams are made up of approximately spherical cells, it can be assumed that the smaller the cell size (at a given foam density), the thinner the Al_2O_3 strut spacing. As a result, a finer microstructure is favoured in terms of prohibiting direct crack propagation through a broad foam strut.

In addition, an investigation into the development of cavities in spherical metal inclusions within Al/Al_2O_3 interpenetrating composites fabricated by gas pressure infiltration [23] showed that cavitations in metal matrix composites can be caused by residual stresses due to

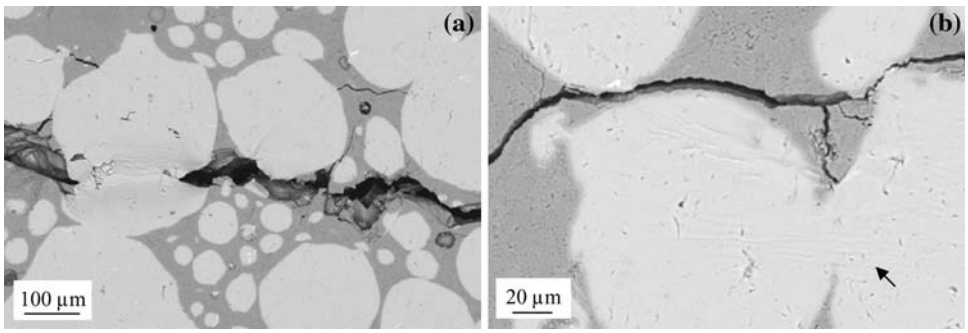

Fig. 7 SEM micrographs of the fractured surface of the Al-8 wt% Mg/Al_2O_3 composite: **a** metal bridging along the crack propagation route, **b** slip bands in the Al in the cells

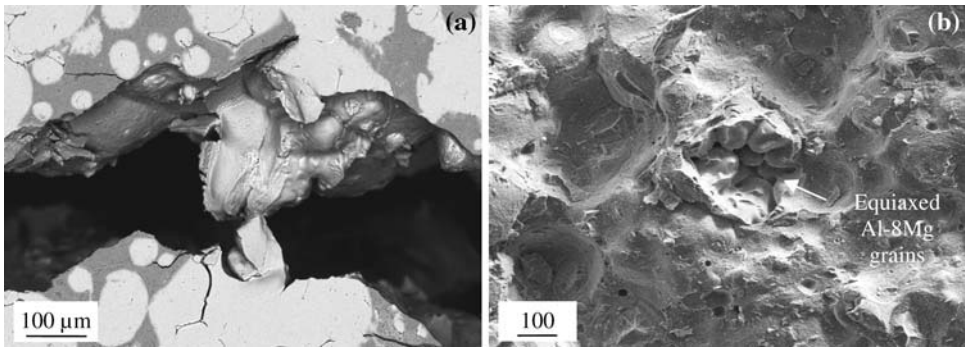

Fig. 8 SEM micrographs of the fractured surfaces of the Al-8 wt% Mg/Al_2O_3 composites: **a** cracks on the Al grain boundaries (back-scattered electron microscopy), **b** crack propagation along the Al grain boundaries (second electron microscopy)

thermal expansion mismatch. The results indicated that the cavities formed preferentially in large metal inclusions and served as fracture origins. In the current research, it has been shown that grain boundaries tend to form in the alloy in particularly large cells (Fig. 1b). Micrographs of the fracture surfaces of the composites containing large cells are shown in Fig. 8. From Fig. 8a, fine cracks are observed along the alloy grain boundaries though the alloy has extensively deformed; from Fig. 8b, equiaxed alloy grains are exposed on the fractured surface of the composite, where fracture occurred along the grain boundaries. Hence, another possible reason for the preference of a smaller cell size is the reduced potential for the formation of cavities or fracture origins, as the intergranular bonding between the alloy grains could be weaker when compared with the strong metal–ceramic interfacial bonding, or micro-shrinkage pores could exist along the Al grain boundaries.

Finally, it has been found that both Mg and N_2 are essential for the pressureless infiltration and play a significant role in providing better metal–ceramic interfacial bonding, hence improved mechanical properties of the composites [19]. However, Mg has a higher coefficient of thermal expansion than that of Al, which could result in microcracking where the Mg is highly concentrated. In addition, Mg can also react to form MgO along the alloy grain boundaries, especially when the Mg content is high; SEM–EDS micrographs of MgO at these grain boundaries and at localised positions at the metal–ceramic interface in an Al-11 wt% Mg/Al_2O_3 composite are shown in Fig. 9. It can be seen that the bonding between the MgO was poor and cracks are present in these regions, which could be harmful to the mechanical properties of the composites. Similarly, excessive exposure to N_2 can result in severe nitridation as mentioned earlier, again this may be detrimental to the mechanical properties as a result of fracture through the brittle AlN layer formed; similar effects due to the formation and fracture of brittle Al_4C_3 in an Al/C_{fiber} composite were observed by Wang et al. [11].

Conclusions

3–3 Al–Mg/Al_2O_3 interpenetrating composites having different Al_2O_3 foam densities and cell sizes have been produced in a N_2 atmosphere by infiltrating 8 wt% Mg content Al–Mg alloy into Al_2O_3 foams with highly interconnected porosity. The microstructure and flexural property of the composites have been characterised. The flexural strength of the Al_2O_3 foams was observed to increase with increasing foam density and decreasing cell size, whilst the strength of the composites increased with both decreasing foam density and cell size—a preference for higher metal content and finer microstructure. Fractural topographic analysis revealed that crack propagates preferentially in the ceramic phase, whilst good metal–ceramic interfacial bonding, metal bridging through plastic deformation and the crack deflection are the main reasons for the high strength.

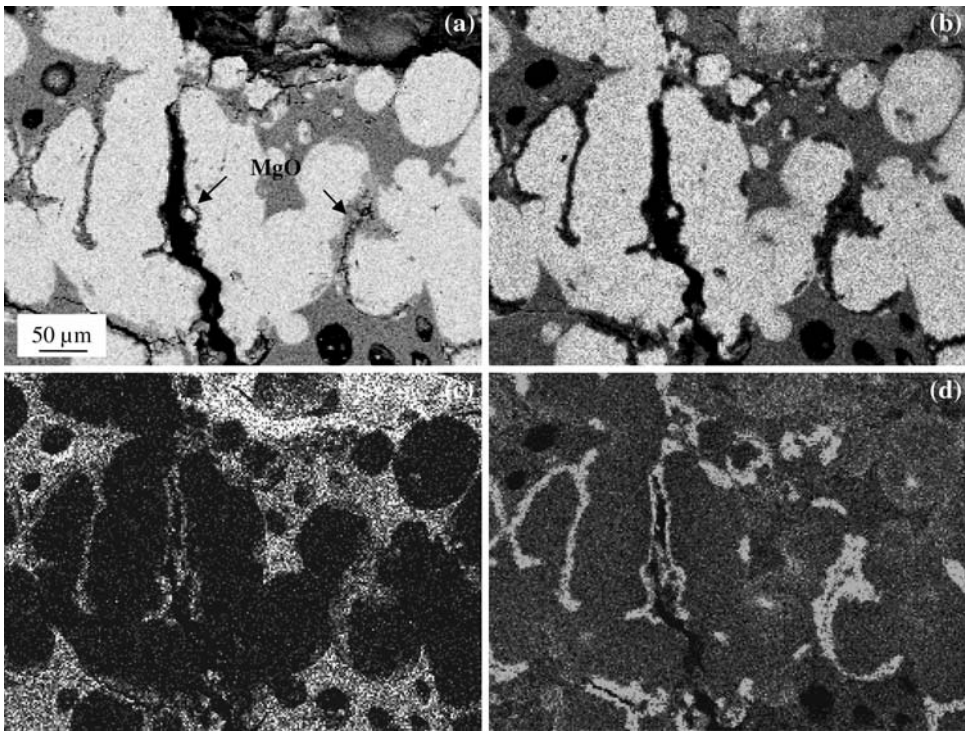

Fig. 9 SEM micrograph and the EDS chemical maps of the Al-11 wt% Mg/Al_2O_3 composites: **a** SEM micrograph, **b** Al, **c** O, **d** Mg

Acknowledgements The authors gratefully acknowledge funding from the EPSRC, UK and Dyson Thermal Technologies, Sheffield, UK, for supplying the alumina foams.

References

1. Bannister M, Shercliff H, Bao G, Zok F, Ashby MF (1992) Acta Metall Mater 40:1531
2. Farber KT, Evans AG (1983) Acta Metall 31:577
3. Evans AG, Cannon RM (1986) Acta Metall 34:761
4. Sigl LS, Mataga PA, Dalgleish BJ, McMeeking RM, Evans AG (1988) Acta Metall 36:945
5. Rödel J (1992) J Eur Ceram Soc 10:143
6. Tuan WH, Pai YP (1999) J Am Ceram Soc 82:1624
7. Lü P, Yue XY, Yu L, Ru HQ (2009) J Mater Sci 44:3483. doi:10.1007/s10853-009-3466-z
8. Luan WZ, Jiang CH, Ji V, Wang HW (2009) J Mater Sci 44:2454. doi:10.1007/s10853-009-3310-5
9. Sadeghian Z, Enayati MH, Beiss P (2009) J Mater Sci 44:2566. doi:10.1007/s10853-009-3335-9
10. Srivastava VC, Rudrakshi GB, Uhlenwinkel V, Ojha SN (2009) J Mater Sci 44:2288. doi:10.1007/s10853-008-2924-3
11. Wang X, Chen GQ, Li B, Wu GH, Jiang DM (2009) J Mater Sci 44:4303. doi:10.1007/s10853-009-3639-9
12. Cheng SL, Yang GC, Wang JC, Yang CL, Zhu M, Zhou YH (2009) J Mater Sci 44:3420. doi:10.1007/s10853-009-3454-3
13. Prielipp H, Knechtel M, Claussen N, Streiffer SK, Müllejans H, Rühle M, Rödel J (1995) Mater Sci Eng A 197:19
14. Skirl S, Krause R, Wiederhorn SM, Rödel J (2001) J Am Ceram Soc 84:2034
15. Klassen T, Günther R, Dickau B, Gärtner F, Bartels A, Bormann R, Mecking H (1998) J Am Ceram Soc 81:2504
16. Clarke DR (1992) J Am Ceram Soc 75:739
17. Binner JGP, Chang H, Higginson RL (2009) J Eur Ceram Soc 29:837
18. Chang H, Binner JGP, Higginson RL (2009) J Microsc 233:132
19. Chang H, Binner JGP, Higginson RL, Sambrook R (2006) Processing of Al-Mg/Al_2O_3 interpenetrating composites by pressureless infiltration. In: Proceedings of the 67th world foundry congress, UK [CD ROM]
20. Zhao LZ, Cao XM, Tian C, Hu WP, Xing HW, Zhang JS (2006) Chin Shu Hsueh Pao 42:325
21. Wang SR, Geng HR, Wang YZ, Zhang JC (2006) Theor Appl Fract Mech 46:57
22. Travitzky NA, Shlayen A (1998) Mater Sci Eng A 244:154
23. Zimmermann A, Hoffman M, Emmel T, Gross D, Rödel J (2001) Acta Mater 49:3177